




Optically active Fe²⁺-doped ZnSe particles in a chalcogenide glass matrix

JUSTIN COOK,¹ MATTHIEU CHAZOT,¹ ALEXANDROS KOSTOGIANNES,¹ RASHI SHARMA,¹ CORBIN FEIT,² JAYNLINN SOSA,² PARAG BANERJEE,² MARTIN RICHARDSON,¹ KATHLEEN A. RICHARDSON,^{1,2} AND KENNETH L. SCHEPLER^{1,*} 

¹CREOL, The College of Optics & Photonics, University of Central Florida, Orlando, FL 32816, USA

²Department of Materials Science and Engineering, University of Central Florida, Orlando, FL 32816, USA

*schepler@creol.ucf.edu

Abstract: High brightness light sources in the mid-infrared are of particular interest for a host of different applications. However, the selection and availability of laser gain media in this spectral region are severely lacking. In this manuscript, we demonstrate broadband optical emission in the 3520-5200 nm region from Fe²⁺-doped ZnSe microparticles dispersed in a chalcogenide glass matrix which is amenable to fiber drawing. A conformal alumina shell was applied to the Fe:ZnSe particles which prevented ZnSe dissolution and preserved normal Fe²⁺ optical absorption and emission properties during the composite material manufacturing process. The broadband emission properties of the Fe:ZnSe-doped chalcogenide glass material observed here are promising for the future development of fiber lasers operating at wavelengths > 4 μm.

© 2022 Optica Publishing Group under the terms of the [Optica Open Access Publishing Agreement](#)

1. Introduction

Mid-infrared (MIR) light (1.5-5 μm) is of interest for numerous applications including medical imaging, medical diagnostics, remote sensing, and infrared countermeasures [1–3]. Fiber lasers offer considerable advantages in this spectral range in terms of size, weight, insensitivity to thermal and vibrational effects, beam quality, flexibility in beam direction and ease of power scaling. However, development of mid-IR fiber lasers is significantly lacking compared with Yb-doped fiber lasers which are routinely operated at multi-kW average powers [4,5]. One issue is that silica-based glasses are no longer low-loss at wavelengths beyond 2 μm [6]. In addition, transition-metal ions (Cr²⁺, Fe²⁺, etc.) capable of mid-IR laser emission require tetrahedral symmetry of the crystal field at the transition-metal ion site, thus typically eliminating glasses as candidate host materials [7].

Despite these concerns, there have recently been several important advances that work towards mitigating these issues in order to realize optical fiber-based laser sources in the MIR. Lasing characteristics have been demonstrated in a 7.5 μm thick Cr²⁺:ZnSe film deposited on sapphire via pulsed laser deposition by Williams et al. [8]. In order to leverage the inherent benefits optical fibers provide, Sparks et al. [9] demonstrated lasing around 2.3 μm with Cr²⁺:ZnSe deposited on the inner surface of a hollow-core silica fiber via high pressure chemical vapor deposition (HPCVD). Similarly, Coco et al. reported continuous wave lasing characteristics from optical fibers with an Fe²⁺:ZnSe core composition fabricated via HPCVD [10]. By using a non-oxide glass chemistry, Xia et al. [11] demonstrated Cr²⁺ emission from Cr²⁺:ZnSe particles embedded in a chalcogenide glass (ChG) fabricated from powders using hot uniaxial pressing (HUP) and melt-quenching methods. More recently, Li et al. [12] investigated the optical properties of Fe²⁺-doped ZnSe microspheres prepared using a solvo-thermal method. Ultra-broadband emission covering the 2.5-5.5 μm has also been observed from Ni²⁺-doped

chalcogenide glass ceramics [13], and several demonstrations of lasers at wavelengths $> 5 \mu\text{m}$ have been reported [14–16]. In addition to these advancements based on solid-core optical fibers and ridge waveguides, gas filled hollow core fibers (HCF) have been used to generate coherent radiation at wavelengths $> 4 \mu\text{m}$ [17,18].

To date, however, no demonstration of any high power/efficiency transition metal doped optical fiber-based laser source has been reported in the literature. To meet the needs of the aforementioned applications, laser sources with at least Watt level average powers are likely required. Among the laser technologies described herein, each has associated obstacles which must be overcome to realize efficient light generation. For hollow-core optical fibers filled via HPCVD, this fabrication method inevitably leads to a hole in the center of the fiber and so far has only demonstrated short fiber lengths [9,10]. On the other hand, HCFs suffer from potential contamination of the fiber interior as well as fabrication and handling difficulties [19,20].

Towards the goal of a high power, mid-IR fiber laser, we report here the development and characterization of an optically active Fe:ZnSe-doped chalcogenide glass composite material which displays broadband emission in the 3.52-5.20 μm range and is amenable to optical fiber drawing. This composite material is appealing for the fabrication of transition metal-doped optical fibers because it enables the ferrous ions to remain in the required tetrahedral configuration within the ZnSe crystals, while also remaining amenable to fiber fabrication as a preform. Synthesis of a composite material consisting of ZnSe microparticles in a chalcogenide matrix has been previously described in [21] and [22]. Here we report fabrication of the composite material using ZnSe particles doped with Fe^{2+} ions. Observation of optical emission from this material indicates that tetrahedrally coordinated Fe^{2+} ions are retained in the ZnSe particles. Optical characteristics of the Fe^{2+} dopant ions remain following incorporation of the particles within a refractive index matched ChG matrix which has previously been deemed suitable for optical fiber fabrication [21]. These findings represent a promising avenue for developing fiber lasers in the $\sim 3.5\text{-}5.5 \mu\text{m}$ band.

2. Sample fabrication

To fabricate the 94.6 As_2S_3 – 5.4 As_2Se_3 ChG base material used in the optically active composite material, the melt quenching technique was employed [21,22]. This ChG composition was chosen specifically to match both the refractive index and dispersion of ZnSe across the wavelength range of interest as well as its capability to form low-loss optical fibers. High purity (5N) raw materials (As, S, Se) were combined in a fused silica ampoule and evacuated to 10^{-2} Torr before being sealed with a hydrogen/oxygen torch. The ampoule was then placed inside a rocking furnace and heated at $1^\circ\text{C}/\text{min}$ up to 750°C and maintained at this temperature for 14 hours. Afterward, the glass was air quenched at 600°C before being annealed at 190°C for 4 hours. After synthesis, the glass was ground using a planetary ball mill in ambient lab conditions and sieved using a sieve shaker. Decreasing sieve sizes of 125 μm , 53 μm and 25 μm were used to size both the ZnSe particles and ChG matrix glass, prior to mixing. Particles with maximum dimensions $\leq 25 \mu\text{m}$ were then used to prepare the Fe:ZnSe-doped chalcogenide composite material.

To prepare the Fe:ZnSe powder, bulk polycrystalline Fe:ZnSe with 10^{19} ions/ cm^3 Fe^{2+} concentration was ground and sieved using a protocol like that used for the ChG base glass (BG) to produce microparticles with dimensions $\leq 25 \mu\text{m}$. Bulk Fe:ZnSe samples were fabricated by researchers at the Air Force Research Laboratory using the hot isostatic pressing (HIP) treatment method [23,24]. Treatment via the HIP process consisted of sputtering a layer of iron onto the surface of commercially available polycrystalline ZnSe disks (25.4 mm diameter, 3 mm thickness) before being placed into the HIP chamber where the temperature and pressure were raised to 1050°C and 30,000 PSI, respectively. During HIP processing, Zn ions were replaced by Fe^{2+} ions via diffusion forming the Fe^{2+} -doped ZnSe material.

After grinding of the HIP treated Fe:ZnSe disks, single gram batches of Fe:ZnSe microparticles were loaded into an atomic layer deposition (ALD) rotatory reactor where thin conformal shells of Al_2O_3 were deposited on the exterior of the microparticles using sequential pulses of TMA and H_2O at 180°C . The purpose of this coating was to prevent dissolution of the ZnSe within the ChG host when the mixture is heated during the ‘remelt’ process to form the composite material. Previous material synthesis performed without the alumina shells showed significant dissolution of the ZnSe particles in the ChG base material during heating of the mixture [21].

After preparation of both ChG and coated Fe:ZnSe powders, the powders were added to a clean fused silica ampoule and mixed at a 5 wt.% Fe:ZnSe loading level before being baked at 150°C for one hour to remove any water vapor which may have been introduced during the grinding/sieving processes. After evacuating the ampoule to 10^{-2} Torr and sealing it with a hydrogen/oxygen torch, the mixture was then heated in a rocking furnace at a rate of $1.8^\circ\text{C}/\text{min}$ up to 650°C which was maintained for up to 8 hours, air quenched at 650°C , and annealed at 190°C for 4 hours. Following removal from the ampoule, the composite material was sliced into a 10 mm diameter, 1.2 mm thick disk and polished to an inspection polish finish, in order to investigate its optical emission properties. Figure 1 illustrates the process flow for particle and composite fabrication used in the present effort. While the handling of powders was maintained in a N_2 purged glove box where possible during the processing of the composite, no additional purification of elemental starting materials and/or glass was carried out to remove impurities.

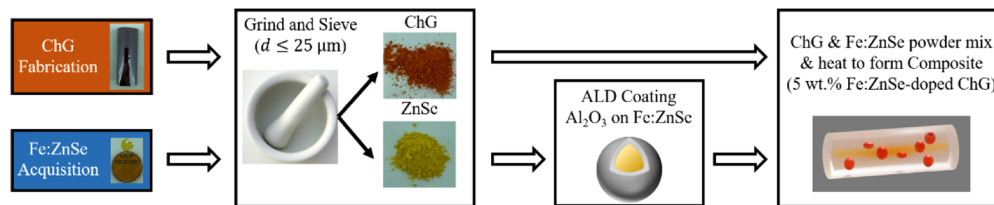


Fig. 1. Flow chart describing the synthesis of the Fe:ZnSe-doped ChG composite materials. After fabrication of the ChG and acquisition of the Fe:ZnSe, both materials are ground and sieved to produce microparticles $\leq 25 \mu\text{m}$ in size. A conformal Al_2O_3 coating is then applied to the Fe:ZnSe powder using atomic layer deposition (ALD). The coated Fe:ZnSe powder is then mixed with the ChG powder at 5 wt.% loading before remelting to form a Fe:ZnSe-doped ChG composite material. Pictures of ALD coating and composite material are conceptual.

3. Optical experimental setup

Figure 2 shows the experimental setup used to characterize the fluorescence emission from the 5 wt.% Fe:ZnSe-doped ChG composite material. The composite material was housed in a liquid nitrogen cooled cryostat outfitted with MgF_2 windows and was held at $\sim 77\text{ K}$ during optical interrogation. A flashlamp pumped Er:YAG laser operating in long pulse mode was used to optically excite the composite material for analysis of the fluorescence spectrum: the pump laser output consisted of 49 mJ, 200 μs pulses at 8 Hz repetition rate with a spectrum centered at 2940 nm. Pump light was then focused onto the Fe:ZnSe-doped ChG composite using an off-axis parabolic mirror ($f = 20\text{ cm}$).

The fluorescence emission from the composite material was then collected using a second off-axis parabolic mirror ($f = 10\text{ cm}$) before being imaged onto the entrance slit of a Czerny-Turner monochromator (Horiba Micro-HR) for spectral analysis. The monochromator utilized a 150 lines/mm ruled diffraction grating and was capable of discriminating signals across the MIR out to $8 \mu\text{m}$. Light transmitted through the monochromator was collected using a 40 mm CaF_2 plano-convex lens and focused onto a mid-IR photodiode (VIGO PVI-5) for signal acquisition.

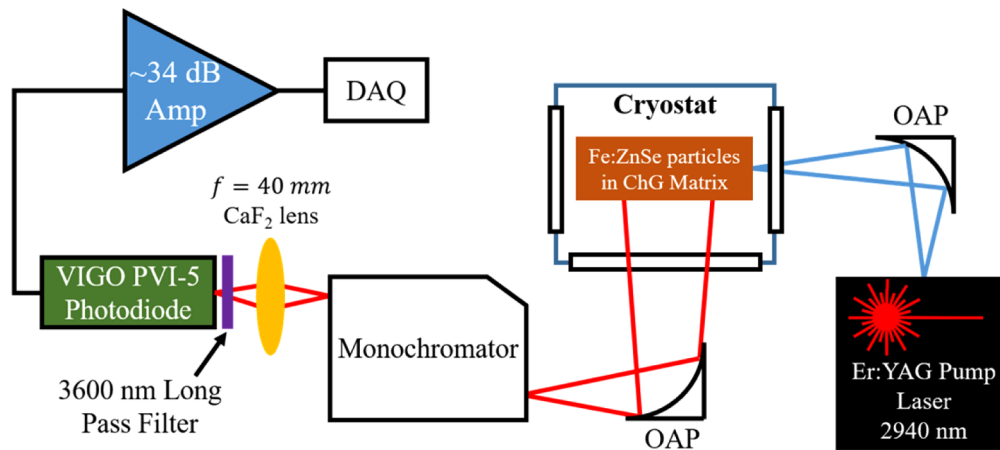


Fig. 2. Optical setup used to measure the fluorescence spectrum of the 5 wt.% Fe:ZnSe-doped ChG composite material. OAP: off-axis parabolic mirror. DAQ: data acquisition. ChG: chalcogenide glass.

This monochromator and photodiode combination enabled reliable measurements of the emission spectrum out to $5.6\ \mu\text{m}$ (no lock-in detection required). To prevent any spurious signal which may arise from stray pump light, a 3600 nm long pass filter (Edmund Optics #33-970) with a measured attenuation of $\sim 27\ \text{dB}$ at the pump wavelength was mounted in front of the photodiode. The signal from the photodiode then passed through a 34 dB electrical amplifier before being recorded on an oscilloscope. It must be noted that while some attenuation at wavelengths $< 3800\ \text{nm}$ was present (due to the spectral response of the long pass filter) and was uncorrected, this experimental setup was consistent across all Fe^{2+} -doped samples measured within this manuscript.

4. Results

4.1. Structural analysis

To validate the observed optical response of the composite, confirmation of behavior of both the dopant Fe:ZnSe powder and ChG matrix was carried out. Key to this was confirmation that the coated Fe:ZnSe powder survived the glass matrix remelt process during composite formation. Figure 3(a) illustrates the x-ray diffraction (XRD) data of both the BG matrix reference and the composite made of 5 wt.% Fe:ZnSe coated powders embedded in a BG matrix. The diffractograms reveal the presence of both ZnSe and ZnS XRD peaks in the composite materials as referenced to the (JCPDS) PDF files of ZnS blende (No. 005-0566) and ZnSe blende (No. 037-1463), where the blue squares and orange stars in Fig. 3(a) correspond to the expected primary x-ray diffraction peaks (2θ) of ZnSe ($\sim 27^\circ$) and ZnS ($\sim 29^\circ$) obtained from the (JCPDS) files, respectively. These data illustrate that despite the application of 300 layers of alumina deposited on the Fe:ZnSe via ALD [25], some of the ZnSe powder has been dissolved during the remelt process. In previous studies we have shown that when not protected with any coating, the ZnSe particles are completely dissolved during the remelt step and that Zn combines with S in the glass matrix to form ZnS crystallites within this sulfur-based glass matrix [21]. As can be seen, the presence of an ALD coating deposited on ZnSe powders, significantly reduces the dissolution of the ZnSe particles, even if a partial dissolution (and re-precipitation of some ZnS) can still be observed. This finding has been attributed to possible breaches in the conformal alumina coating (which is nominally $\sim 25\text{-}35\ \text{nm}$ thick) which can occur when particles agglomerate

into soft clusters during ALD processing [21]. Transmission electron microscopy (TEM) data substantiates this result, confirming that some of the powders were not fully coated, and explains why dissolution was observed, as evidenced in the ZnS diffraction peaks for the optical composite shown in Fig. 3(a). However, the presence of ZnSe peaks after the long remelt (6 hours) is excellent evidence as to the effectiveness of the Al_2O_3 coating to protect the iron doped particles.

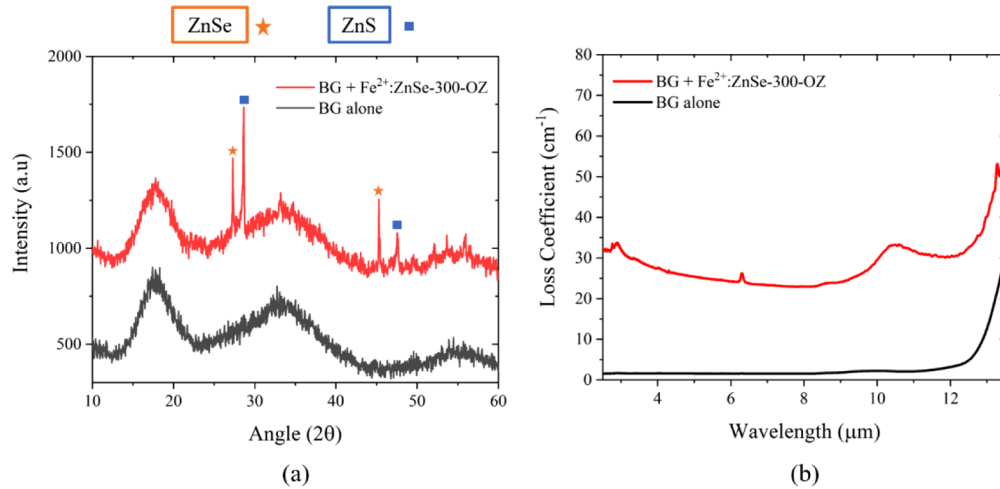


Fig. 3. (a) Bulk XRD pattern and (b) FTIR spectra of BG and Fe:ZnSe-doped composite materials. Bulk sample thicknesses were 2.1 mm for the BG and 1.2 mm for the Fe:ZnSe-doped composite, respectively.

Figure 3(b) shows the measured loss spectra of the BG and the Fe:ZnSe doped BG composite material. Several extrinsic absorption bands can be observed attributed largely to impurities associated with moisture. These absorptions are specifically related to hydride, hydroxide and oxide compounds. The most important bands that can be observed can be ascribed to: $-\text{O}-\text{H}^-$ at 2.92 μm ; $-\text{S}-\text{H}$ at 4.0 μm (weak); H_2O at 6.3 μm ; $-\text{As}-\text{O}$ at 8.9 μm and 9.5 μm ; and $-\text{Se}-\text{O}$ at 10.1 μm . The IR spectrum of the composite is also dominated by a strong overall absorbance due to scattering losses. This is likely directly linked to the formation of ZnS micro-crystals in the material during the remelt process which results in strong Mie-scattering losses due to the refractive index mismatch of ZnS with that of the As-S-Se BG matrix. The index mismatch of the alumina shell is expected to cause little scattering due to the subwavelength thickness (~ 35 nm) of the shell. Additionally, TEM and second harmonic generation (SHG) microscopy (used to evaluate particle survival following remelt, alumina shell coating thickness and post-remelt Fe:ZnSe agglomerate size) confirm the particles are large (on the order of 45-55 μm) [26]. As this effort aimed to demonstrate proof of concept of our approach, no effort was made to reduce this particle size further, nor to remove moisture-related impurities known to be present in the base glass matrix.

4.2. Optical characterization

Figure 4 details the structural and spectroscopic properties of Fe:ZnSe which are relevant to emission in the mid-IR. Fe:ZnSe features a tetrahedral crystal structure where Fe^{2+} ions replace Zn^{2+} ions within the crystal lattice, as shown in Fig. 4(a). Due to the tetrahedral symmetry, the ^5D ground state of Fe^{2+} is split into the electronic ^5E and $^5\text{T}_2$ sublevels. This crystal field splitting, in addition to the coupling between the electronic sublevels and the vibrational modes of ZnSe, results in broadband optical transitions in the 2.5-5.5 μm spectral region (Fig. 4(b)) [27]. The absorption and emission cross-sections corresponding to these transitions measured in a bulk

Fe:ZnSe sample are shown in Fig. 4(c) and indicate spectrally broadband absorption and emission features which are suitable for lasing [28]. In particular, the broad emission band shown in Fig. 4(c) extending from ~ 3.5 - $5.5 \mu\text{m}$ is of interest for developing mid-IR optical fiber-based laser sources and is subject to current investigation for the Fe:ZnSe-doped ChG composite material presented within this manuscript.

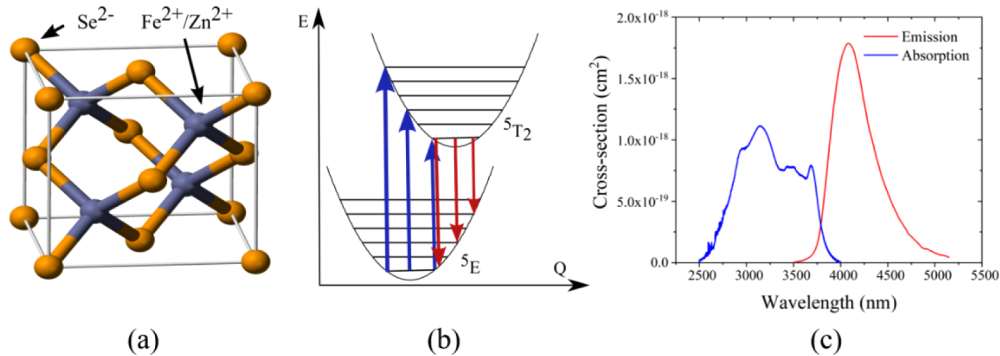


Fig. 4. (a) Tetrahedral structure of Fe:ZnSe after HIP treatment in which Fe²⁺ ions are substituted for Zn²⁺. (b) Energy level structure of Fe²⁺ ions in ZnSe. The ⁵D ground state is split into the ⁵E and ⁵T₂ sublevels as a result of the tetrahedral crystal field. Allowed optical transitions are shown in blue and red, corresponding to various absorption and emission wavelengths respectively. (c) Measured absorption (blue) and emission (red) cross-sections for Fe²⁺ ions in ZnSe at 77 K. Cross-section data was adapted from [28].

To determine the emission properties of Fe²⁺ doped optical materials, the experimental setup shown in Fig. 2 was employed. Using this setup, the fluorescence signal was measured at ~ 77 K, both as a function of time and wavelength. Figure 5(a) shows the temporal evolution of the emission signal (black) as well as the input Er:YAG pump pulse (green). A robust signal was observed emanating from the 5 wt.% composite material, indicating emission was occurring from the Fe²⁺ ions within the composite matrix. However, due to the long pulse duration ($\sim 200 \mu\text{s}$) of the Er:YAG pump laser relative to the upper-state lifetime of Fe²⁺ ions, an accurate lifetime measurement could not be performed on the 5 wt.% composite material.

To further evaluate the fluorescence signal, the emission spectrum measured at ~ 77 K from both the 5 wt.% composite material (black) and a bulk Fe:ZnSe polycrystalline reference sample (red) [23] are shown in Fig. 5(b). Broadband emission covering the 3520-5200 nm spectral region was observed from the composite material, indicating the presence of optically active Fe²⁺ ions. In comparison, the emission spectrum of the bulk Fe:ZnSe reference sample is shown in red, indicating emission ranging from 3560-5240 nm. The strong dip in the emission spectrum of both samples observed around $4.2 \mu\text{m}$ was due to absorption by atmospheric CO₂.

Comparing the composite material data against that obtained from the bulk Fe:ZnSe sample shows a significant peak at 3840 nm in the emission spectrum of the composite sample. The shift from the bulk peak at 4080 nm is similar to the shift of the peak emission wavelength in Fe:ZnS compared to Fe:ZnSe [29]. As indicated in the X-ray structural analysis, some of the ZnSe particles dissolved or partially dissolved and recrystallized as ZnS. Fe²⁺ ions may be substituting into the ZnS crystals as they crystallize. On the other hand, a shoulder peak at 3840 nm is also present in the bulk sample. Thus, an alternative explanation could be related to the size of the individual crystallites; near-surface crystal field effects would be stronger in the smaller ZnSe particles present in the composite. We also considered the possibility of impurity absorption in the $4 \mu\text{m}$ region (e.g. -S-H) but the bulk ZnSe starting material is not expected to have significant impurities and we see the $4 \mu\text{m}$ dip in both bulk and composite samples. Finally, we considered

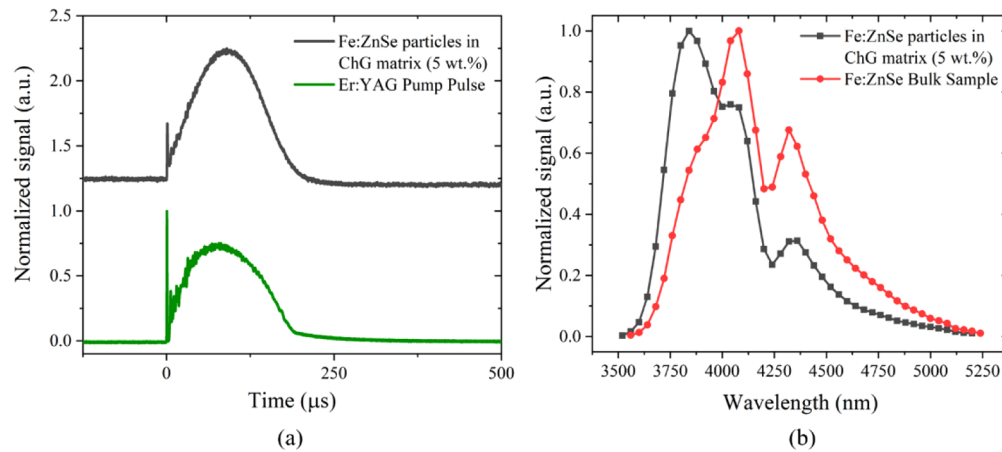


Fig. 5. (a) Temporal evolution of the 5 wt.% Fe:ZnSe-doped ChG composite emission signal (black) and Er:YAG pump pulse (green). (b) Measured fluorescence spectrum from the 5 wt.% Fe:ZnSe-doped ChG composite (black) and a bulk Fe:ZnSe crystal (red) used as a reference source.

the possibility of blue shifting being due to diffusion of iron out of the ZnSe particles (less Fe²⁺ concentration in the ZnSe resulting in less self-absorption) but saw no spectroscopic evidence of iron in the glass. The explanation for the blue shifted peak needs further investigation.

Finally, it is important to note that the Fe²⁺ emission signal from the composite material was similar in order of magnitude to that of the bulk material even though the Fe:ZnSe particle loading in the glass was only 5%. Also, despite no purification steps during composite fabrication and high scattering loss in the composite material, the emission signal was easily observed, making these results promising for future development of fiber laser sources operating at > 4 μm based on this Fe:ZnSe-doped ChG composite material.

5. Conclusion

We have successfully fabricated composites of Fe²⁺-doped ZnSe microparticles dispersed in a refractive index-matched chalcogenide glass which are amenable to optical fiber fabrication and evaluated their optical behavior. Optical emission characteristic of Fe²⁺ ions in a tetrahedral crystal field was observed when pumping at 2940 nm. This proof of Fe²⁺ optical activity after the mixing and remelting process is an encouraging step towards our goal of demonstrating mid-IR fiber laser operation based on this composite material.

The observation of strong Fe²⁺ emission in the composite sample, in spite of agglomeration-induced scattering loss, known base glass matrix impurities and partial dissolution of the Fe:ZnSe particles, bodes well for further progress towards the realization of a low loss, optical composite preform, suitable for fiber drawing. We continue efforts to improve the quality of our conformal ALD alumina shell coating by employing modifications to deposition chemistries which are expected to reduce ZnSe dissolution. Additionally, these refinements to the ALD process chemistry will reduce particle agglomeration and aid in enhanced dispersion within the preform matrix. Lastly, progress in handling protocols to further reducing impurity losses enabling fabrication of low loss fiber will provide demonstration of the end goal of an active fiber.

Funding. Air Force Office of Scientific Research (FA9550-19-1-0127).

Acknowledgments. We thank Gary Cook and Sean McDaniel at the Air Force Research Laboratory, Wright-Patterson AFB for preparing the iron doping of bulk ZnSe samples for us.

Disclosures. The authors declare no conflicts of interest.

Data Availability. Data underlying the results presented in this paper are not publicly available at this time but may be obtained from the authors upon reasonable request.

References

1. M. Weida, E. Fotheringham, W. Chapman, and T. Day, "Progress towards compact broadly tunable laser modules for high-resolution mid-IR spectroscopy and commercial applications," *Proc. SPIE* **8268**, 82682I (2012).
2. A. Sijan, "Development of military lasers for optical countermeasures in the mid-IR," *Proc. SPIE* **7483**, 748304 (2009).
3. A. R. Adams, C. T. Elliott, A. Krier, B. N. Murdin, R. W. Waynant, I. K. Ilev, and I. Gannot, "Mid-infrared laser applications in medicine and biology," *Philos. Trans. R. Soc., A* **359**(1780), 457–458 (2001).
4. M. Lemieux-Tanguay, V. Fortin, T. Boilard, P. Paradis, F. Maes, L. Talbot, R. Vallée, and M. Bernier, "15 W monolithic fiber laser at 3.55 μm ," *Opt. Lett.* **47**(2), 289–292 (2022).
5. Y. O. Aydin, V. Fortin, R. Vallée, and M. Bernier, "Towards power scaling of 2.8 μm fiber lasers," *Opt. Lett.* **43**(18), 4542–4545 (2018).
6. C. B. Layne, W. H. Lowdermilk, and M. J. Weber, "Multiphonon relaxation of rare-earth ions in oxide glasses," *Phys. Rev. B* **16**(1), 10–20 (1977).
7. L. D. DeLoach, R. H. Page, G. D. Wilke, S. A. Payne, and W. F. Krupke, "Transition metal-doped zinc chalcogenides: spectroscopy and laser demonstration of a new class of gain media," *IEEE J. Quantum Electron.* **32**(6), 885–895 (1996).
8. J. E. Williams, V. V. Fedorov, D. V. Martyshev, I. S. Moskalev, R. P. Camata, and S. B. Mirov, "Mid-IR laser oscillation in Cr^{2+} :ZnSe planar waveguide," *Opt. Express* **18**(25), 25999–26006 (2010).
9. J. R. Sparks, S. C. Aro, R. He, M. L. Goetz, J. P. Krug, S. A. McDaniel, P. A. Berry, G. Cook, K. L. Schepler, P. J. Sazio, V. Gopalan, and J. V. Badding, "Chromium doped zinc selenide optical fiber lasers," *Opt. Mater. Express* **10**(8), 1843–1852 (2020).
10. M. G. Coco, S. C. Aro, S. A. McDaniel, A. Hendrickson, J. P. Krug, P. J. Sazio, G. Cook, V. Gopalan, and J. V. Badding, "Continuous wave Fe^{2+} :ZnSe mid-IR optical fiber lasers," *Opt. Express* **28**(20), 30263–30274 (2020).
11. K.-L. Xia, G. Jia, H.-T. Gan, Y.-M. Gui, X.-S. Zhang, Z.-J. Liu, and X. Shen, "Ultrabroadband mid-infrared emission from Cr^{2+} :ZnSe-doped chalcogenide glasses prepared via hot uniaxial pressing and melt-quenching*," *Chin. Phys. B* **30**(9), 094208 (2021).
12. T. Li, C. Sun, C. Xue, Y. Jiang, J. Zhang, and L. Zhao, "Structure and optical properties of iron doped ZnSe microspheres," *Opt. Mater.* **114**, 110989 (2021).
13. M. Cui, A. Yang, M. Sun, H. Lin, H. Lin, J. Ren, and Z. Yang, "2.5–5.5 μm mid-infrared emission from Ni^{2+} -doped chalcogenide glass ceramics containing CsPbI_3 perovskite nanocrystals," *J. Am. Ceram. Soc.* **104**(11), 5593–5598 (2021).
14. V. S. Shiryaev, M. V. Sukhanov, A. P. Velmuzhov, E. V. Karaksina, T. V. Kotereva, G. E. Snopatin, B. I. Denker, B. I. Galagan, S. E. Sverchkov, V. V. Koltashev, and V. G. Plotnichenko, "Core-clad terbium doped chalcogenide glass fiber with laser action at 5.38 μm ," *J. Non-Cryst. Solids* **567**, 120939 (2021).
15. J. J. Nunes, L. Sojka, R. W. Crane, D. Furniss, Z. Q. Tang, D. Mabwa, B. Xiao, T. M. Benson, M. Farries, N. Kalfagiannis, E. Barney, S. Phang, A. B. Seddon, and S. Sujecki, "Room temperature mid-infrared fiber lasing beyond 5 μm in chalcogenide glass small-core step index fiber," *Opt. Lett.* **46**(15), 3504–3507 (2021).
16. P. Fjodorow, M. P. Frolov, S. O. Leonov, B. I. Denker, B. I. Galagan, S. E. Sverchkov, V. V. Koltashev, V. G. Plotnichenko, M. V. Sukhanov, and A. P. Velmuzhov, "Mid-infrared laser performance of Ce^{3+} -doped selenide glass," *Opt. Express* **29**(17), 27674–27682 (2021).
17. A. Pryamikov, "Gas fiber lasers may represent a breakthrough in creating powerful radiation sources in the mid-IR," *Light: Sci. Appl.* **11**(1), 36 (2022).
18. F. B. A. Aghbolagh, V. Nampoothiri, B. Debord, F. Gerome, L. Vincetti, F. Benabid, and W. Rudolph, "Mid IR hollow core fiber gas laser emitting at 4.6 μm ," *Opt. Lett.* **44**(2), 383–386 (2019).
19. I. Gris-Sanchez and J. C. Knight, "Time-dependent degradation of photonic crystal fiber attenuation around OH absorption wavelengths," *J. Lightwave Technol.* **30**(23), 3597–3602 (2012).
20. Y. Min, A. Filipkowski, G. Stepniowski, D. Dobrakowski, J. Zhou, B. Lou, M. Klimczak, L. Zhao, and R. Buczyński, "Fusion splicing of silica hollow core anti-resonant fibers with polarization maintaining fibers," *J. Lightwave Technol.* **39**(10), 3251–3259 (2021).
21. M. Chazot, C. Arias, M. Kang, C. Blanco, A. Kostogiannes, J. Cook, A. Yadav, V. Rodriguez, F. Adamietz, D. Verreault, S. Danto, T. Loretz, A. Seddon, D. Furniss, K. Schepler, M. C. Richardson, and K. A. Richardson, "Investigation of ZnSe stability and dissolution behavior in As-S-Se chalcogenide glasses," *J. Non-Cryst. Solids* **555**, 120619 (2021).
22. M. Chazot, A. Kostogiannes, M. Julian, C. Feit, J. Sosa, M. Kang, C. Blanco, J. Cook, V. Rodriguez, F. Adamietz, D. Verreault, P. Banerjee, K. Schepler, M. C. Richardson, and K. A. Richardson, "Enhancement of ZnSe stability during optical composite processing via atomic layer deposition," *J. Non-Cryst. Solids* **576**, 121259 (2022).
23. R. W. Stites, S. A. McDaniel, J. O. Barnes, D. M. Krein, J. H. Goldsmith, S. Guha, and G. Cook, "Hot isostatic pressing of transition metal ions into chalcogenide laser host crystals," *Opt. Mater. Express* **6**(10), 3339–3353 (2016).

24. J. W. Evans, R. W. Stites, and T. R. Harris, "Increasing the performance of an Fe:ZnSe laser using a hot isostatic press," *Opt. Mater. Express* **7**(12), 4296–4303 (2017).
25. C. Feit, J. Sosa, A. Kostogiannes, R. Sharma, M. Chazot, K. A. Richardson, and P. Banerjee, "Surface chemistry of ZnSe for efficient nucleation and growth of ALD Al₂O₃," *ACS Appl. Mater. Interfaces* (to be submitted) (2022).
26. M. Chazot, K. A. Richardson, and V. Rodriguez, "SHG Microscopy as a tool to assess composite microstructures," in preparation (2022).
27. J. W. Evans, T. R. Harris, B. R. Reddy, K. L. Schepler, and P. A. Berry, "Optical spectroscopy and modeling of Fe²⁺ ions in zinc selenide," *J. Lumin.* **188**, 541–550 (2017).
28. J. W. Evans, "Iron-doped Zinc Selenide: Spectroscopy and Laser Development," Air Force Institute of Technology and Air Force Air University, AFIT-ENP-DS-14-M-01 (2014).
29. N. Myoung, V. V. Fedorov, S. B. Mirov, and L. E. Wenger, "Temperature and concentration quenching of mid-IR photoluminescence in iron doped ZnSe and ZnS laser crystals," *J. Lumin.* **132**(3), 600–606 (2012).